Optical Materials 36 (2014) 1002–1005

Contents lists available at ScienceDirect

Optical Materials

journal homepage: www.elsevier.com/locate/optmat

Optoelectronic properties of three dimensional WO_3 nanoshale and its application for UV sensing

Dali Shao [a,*], Mingpeng Yu [b,c], Jie Lian [b], Shayla Sawyer [a]

[a] Department of Electrical, Computer, and Systems Engineering, Rensselaer Polytechnic Institute, Troy, NY 12180, USA
[b] Department of Mechanical, Aerospace, and Nuclear Engineering, Rensselaer Polytechnic Institute, Troy, NY 12180, USA
[c] Department of Chemistry, Tsinghua University, Beijing 100084, China

ARTICLE INFO

Article history:
Received 17 September 2013
Accepted 9 January 2014
Available online 30 January 2014

Keywords:
UV photodetector
Tungsten oxide
Responsivity
Photoluminescence

ABSTRACT

A novel three dimensional (3D) WO_3 nanoshale structure was synthesized using a facile hydrothermal synthesis procedure. The structural and optoelectronic properties of the 3D WO_3 nanoshale were characterized by scanning electron microscopy, high resolution transmission electron microscopy, X-ray diffraction, Raman spectroscopy, UV–Vis absorption and photoluminescence measurements. An UV photodetector fabricated from the 3D WO_3 nanoshale showed a good photoresponsivity (5.1 A/W), which is attributed to internal gain that introduced by surface oxygen adsorption–desorption process, as well as high surface to volume ratio of the 3D nanoshale structure. The results in this work may open up new possibilities of using WO_3 for optoelectronic applications including optical switches and photodetectors.

© 2014 Elsevier B.V. All rights reserved.

1. Introduction

WO_3 is an n-type wide bandgap semiconductor material and has excellent electrochromic, optochromic, and gasochromic properties [1–3]. Because of these promising material properties, WO_3 nanostructures have been investigated for various applications including gas sensors, environmental protection and energy conversion [4–6]. However, currently no work systematically investigated the optoelectronic properties of WO_3. UV photodetectors have various commercial and military applications, such as secure space-to-space communications, pollution monitoring, water sterilization, flame sensing and early missile plume detection [7]. To date, many different wide bandgap semiconductors such as GaN, ZnO, Si_3N_4, and In_2O_3 nanostructures have been investigated for UV photodetector applications [8–12]. WO_3 has the potential for UV sensing because of its wide bandgap (~3.3 eV). Therefore, investigation of the optoelectronic properties of new WO_3 nanostructures is desirable for designing high performance UV photodetectors.

In this work, a facile hydrothermal synthesis procedure was developed for synthesis of novel 3D WO_3 nanoshale material. An UV photodetector was fabricated from the 3D WO_3. Due to the internal gain that introduced by surface oxygen adsorption–desorption process and the high surface to volume ratio of the nanoshale structure, the UV photodetector showed a good photoresponsivity in UV region.

2. Experimental

2.1. Synthesis

3D WO_3 nanoshale structure was grown using an *in situ* hydrothermal process. In this process, 0.8 g $Na_2WO_4{\cdot}2H_2O$ and 0.15 g NaCl were dissolved in deionized water and kept stirring for 6 h. Then, 2 M hydrochloric acid solution was added dropwise to the above solution until the pH of the solution was adjusted to approximate 3.0. After that, the solution was transferred into a Teflon-lined stainless steel autoclave (Parr, 4744) and heated to 180 °C. After 15 h hydrothermal treatment, the autoclave was cooled down to room temperature naturally. The precipitate was centrifuged, washed with ethanol and deionized water 6 times and finally dried at 60 °C under vacuum for further characterization.

2.2. Device fabrication

The UV photodetector was fabricated by deposition of 3D WO_3 nanoshale on quartz substrate via spin casting deposition method. Then, interdigitated Al contacts with thickness of 350 nm were deposited on the top using electron beam evaporator. Finally, the photodetector was packaged and wire bonded using Epo-Tek H20E conductive epoxy. The schematic of the UV photodetector is shown in Fig. 1.

2.3. Measurement

The morphology and microstructure of the 3D WO_3 nanoshale structure was characterized by a dual beam scanning electron

* Corresponding author. Tel.: +1 4795954931.
E-mail address: shaod@rpi.edu (D. Shao).

0925-3467/$ - see front matter © 2014 Elsevier B.V. All rights reserved.
http://dx.doi.org/10.1016/j.optmat.2014.01.010

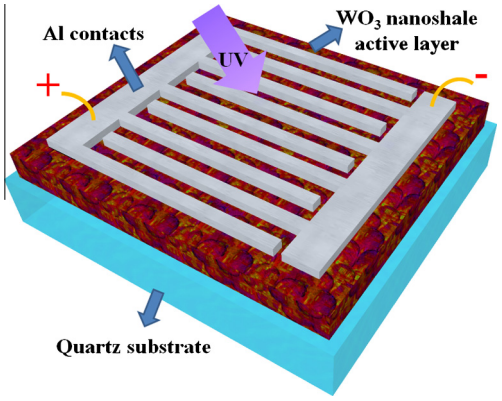

Fig. 1. The schematic of the UV photodetector fabricated from 3D WO_3 nanoshale.

microscopy (SEM, Carl Zeiss Ultra 1540). The crystal structure of the 3D WO_3 nanoshale was confirmed using a high resolution transmission electron microscopy (HRTEM, JEOL 2011). The X-ray diffraction (XRD, PANalytical) patterns was measured at room temperature with Cu Kα radiation (wavelength = 1.54 Å). The chemical state of the WO_3 nanoshale was characterized by X-ray photoelectron spectroscopy (XPS, PHI 5000 Versa Probe). The photoluminescence (PL) spectrum of the 3D WO_3 nanoshale was performed using Spex-Fluorolog-Tau-3 spectrofluorimeter with excitation wavelength fixed at 330 nm. The absorption spectrum of the 3D WO_3 nanoshale was measured using Shimadzu UV–Vis 2550 spectrophotometer with a deuterium lamp (190–390 nm) and a halogen lamp (280–1100 nm). The typical *I*–*V* characteristics and photoresponsivity of the photodetector fabricated from 3D WO_3 nanoshale were measured using a HP4155B semiconductor parameter analyzer and a Shimadzu UV–Vis 2550 spectrophotometer in connection with a Newport 1928-C optical power meter, respectively.

3. Results and discussion

The SEM images of the 3D WO_3 nanoshale structure are shown in Fig. 2a and b and the HRTEM image of the WO_3 nanoshale is shown in the inset of Fig. 1b. It can be seen clearly from Fig. 2b that the 3D WO_3 nanoshale structure has high surface to volume ratio, which is favorable for photodetector and gas sensing applications. The space of the lattice fringes is 0.385 nm, corresponding to the (001) plane of the WO_3 hexagonal cell. This indicates that the 3D WO_3 nanoshale structure is grown along the *c*-axis direction [13].

Fig. 2c shows the X-ray diffraction (XRD) patterns of the 3D WO_3 nanoshale. All the peaks can be well indexed to hexagonal structure of WO_3 (JCPDS 75-2187) with the space group P6/mmm. Fig. 2d shows the W 4f core-level spectrum for the 3D WO_3 nanoshale structure measured by XPS. Two major peaks for W $4f_{7/2}$ and W $4f_{5/2}$ were observed at 35.6 and 37.8 eV, respectively. These results are consistent with the previous report, indicating stoichiometric WO_3 in the nanoshale structure [14].

The room-temperature UV–Vis absorption and photoluminescence spectra of the 3D WO_3 nanoshale structure are shown in Fig. 3. When excited at 330 nm, the PL spectrum of the 3D WO_3 nanoshale structure shows a UV emission band centered at 381 nm and a broad visible emission band with peak wavelength

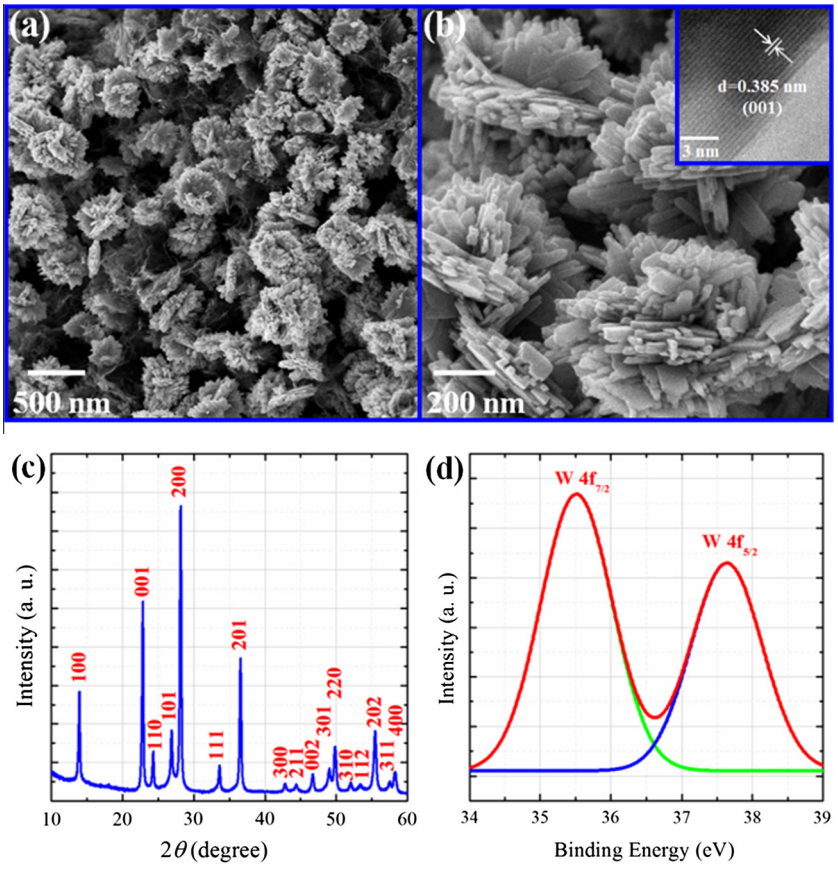

Fig. 2. SEM images of the 3D WO_3 nanoshale structure with (a) medium magnification and (b) high magnification. Inset: HRTEM image of the 3D WO_3 nanoshale material (c) XRD pattern and (d) W 4f peaks of the 3D WO_3 nanoshale structure.

at 437 nm. The inset of Fig. 3 illustrates the PL mechanism of the 3D WO_3 nanoshale. The UV emission band is attributed to the near band-edge emission of the WO_3 crystal while the broad visible emission band is defect level emission that originates from oxygen vacancies in the structure [15].

The typical *I–V* characteristics of the photodetector were measured under dark environment and under 335 nm UV illuminations with varying light intensity, as shown in Fig. 4a. The UV photoconduction mechanism of the 3D WO_3 nanoshale structure is shown in Fig. 4b. The initial low conductivity of the 3D WO_3 nanoshale in dark environment is attributed to surface adsorbed oxygen molecules, which capture the free electrons from WO_3 nanoshale to form negative charged oxygen ions layer $[O_2(g) + e^- \rightarrow O_2^-(ad)]$. This process results formation of a low conductivity depletion region near the surface. The oxygen adsorption process usually happens on the surface oxygen vacancy sites, which is common to metal oxide nanostructures because of incomplete oxidation and imperfect crystallization. Several theoretical predictions indicate that surface defects such as oxygen vacancies often dominate the electronic/chemical properties and adsorption behaviors of metal oxide materials [16]. Upon UV illumination, electron–hole pairs are generated in WO_3 nanoshale structure. The photogenerated holes can migrate to the surface of WO_3 nanoshale and recombine with the negative charged oxygen ions $[h^+ + O_2^-(ad) \rightarrow O_2(g)]$, which result a decrease in the width of the depletion region and an increase in the conductivity of the WO_3 nanoshale. Therefore, the surface oxygen molecule adsorption and desorption process introduce internal gain inside the WO_3 nanoshale structure. This surface oxygen molecule related internal gain mechanism has also been reported for other metal oxide materials such as ZnO and In_2O_3 [17,18].

The transient response of the photodetector is shown in Fig. 5, which was measured by turning on and off a UV light emitting diode with peak wavelength at 335 nm. The rise time (from 10% to 90%) and fall time (from 90% to 10%) of the photodetector were measured to be 6.3 s and 0.5 s, respectively. It is worth to mention that the transient response of the device may be further improved by coating a thin layer of graphene outside the WO_3 nanoshale through a facile three-step method reported in our previous work [19]. However, the coating of a thin graphene layer will inevitably increase the dark current of the device. Therefore, it is important to find a balance point between the transient response and the photocurrent to dark current ratio of the device. Further optimization of the photodetector is underway.

The photoresponsivity of the photodetector, defined as photocurrent per unit of incident optical power, is shown in Fig. 6. A maximum photoresponsivity of 5.1 A/W at 376 nm was observed

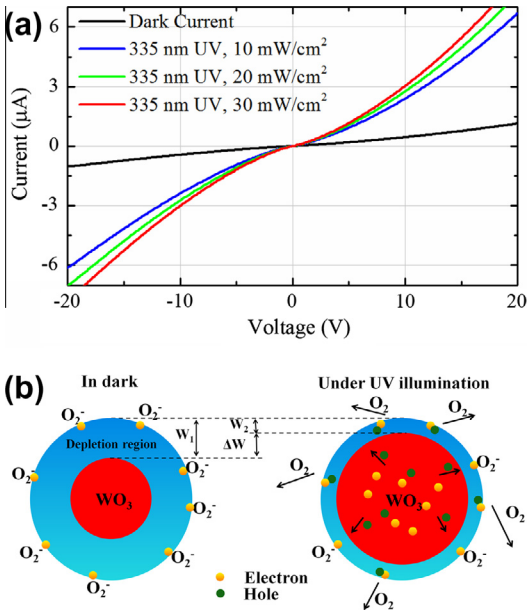

Fig. 4. (a) Typical *I–V* characteristics of the UV photodetector fabricated from the 3D WO_3 nanoshale structure photocurrent was measured with varying light intensity and (b) schematic illustration showing the photoconduction mechanism of the 3D WO_3 nanoshale.

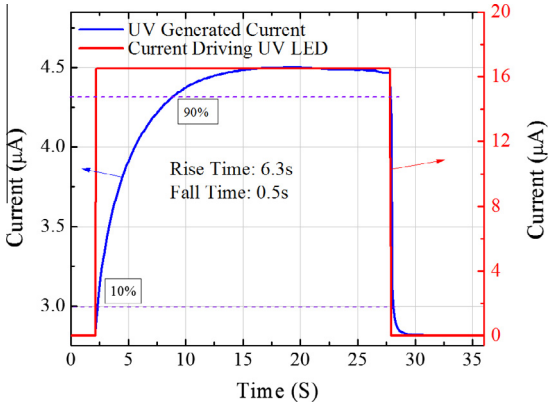

Fig. 5. Transient response of the UV photodetector fabricated from the 3D WO_3 nanoshale structure.

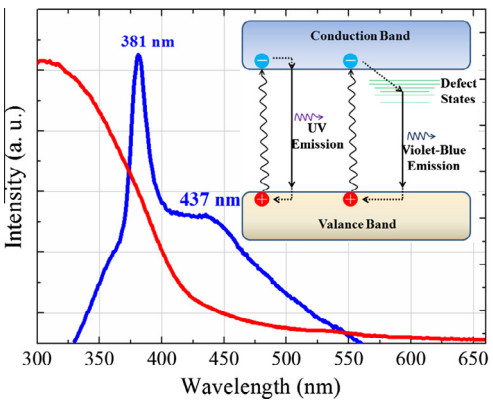

Fig. 3. Absorption and photoluminescence spectra of the 3D WO_3 nanoshale structure.

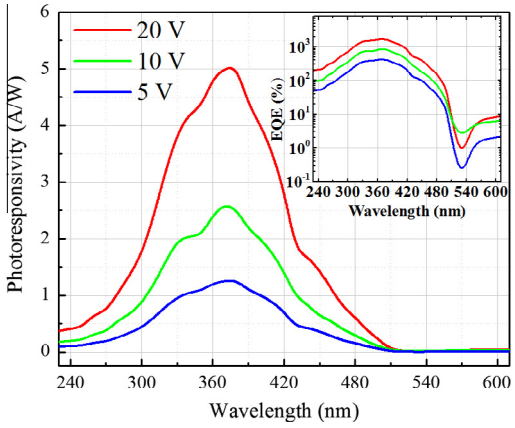

Fig. 6. Photoresponsivity spectra of the UV photodetector fabricated from the 3D WO_3 nanoshale structure. Inset: calculated EQE of the UV photodetector.

under 20 V, which is more than 25 times higher than those of commercial GaN or SiC photodetectors (~0.2 A/W) [20]. The inset of Fig. 6 shows the external quantum efficiency (EQE) of the photodetector calculated using the equation: EQE = $R \times h\nu/q$, where $h\nu$ is the energy of the incident photon in electron volts, q is the electron charge and R is the photoresponsivity of the UV photodetector. The maximum EQE is calculated to be 1678% at 376 nm. Such a high EQE of the UV photodetector, as discussed earlier, is mainly attributed to internal gain that introduced by the oxygen adsorption/desorption process at the surface of WO_3 nanoshale structure.

4. Conclusion

In conclusion, we synthesized a novel 3D WO_3 nanoshale structure using a facile hydrothermal procedure. An UV photodetector fabricated from the 3D WO_3 nanoshale showed good photoresponsivity (5.1 A/W), which is attributed to internal gain that introduced by surface oxygen adsorption–desorption process, as well as high surface to volume ratio of the 3D nanoshale structure. The good material properties of the 3D WO_3 nanoshale demonstrated in this work may open up new possibilities for using WO_3 for future optoelectronic applications such as photodetectors and optical switches.

Acknowledgements

The authors gratefully acknowledge support from National Security Technologies through NSF Industry/University Cooperative Research Center Connection One. The authors also acknowledge the National Science Foundation Smart Lighting Engineering Research Center (EEC-0812056) and a NSF career award DMR 1151028.

References

[1] K. Huang, Q. Zhang, F. Yang, D. He, Nano Res. 3 (2010) 281.
[2] R.R. Kharade, S.P. Patil, R.M. Mane, P.S. Patil, P.N. Bhosale, Opt. Mater. 34 (2011) 322.
[3] R. Sivakumar, R. Gopalakrishnan, M. Jayachandran, C. Sanjeeviraja, Opt. Mater. 29 (2007) 679.
[4] L. Li, Y. Zhang, X. Fang, T. Zhai, M. Liao, X. Sun, Y. Koide, Y. Bando, D. Golberg, J. Mater. Chem. 21 (2011) 6525.
[5] X. An, J.C. Yu, Y. Wang, Y. Hu, X. Yu, G. Zhang, J. Mater. Chem. 22 (2012) 8525.
[6] D. Shao, M. Yu, J. Lian, S. Sawyer, Nanotechnology 24 (2013) 295701.
[7] T.V. Blank, Y.A. Gol'dberg, Semiconductors 37 (2003) 999.
[8] D. Li, X. Sun, H. Song, Z. Li, Y. Chen, H. Jiang, G. Miao, Adv. Mater. 24 (2012) 845.
[9] D. Shao, M. Yu, J. Lian, S. Sawyer, Appl. Phys. Lett. 101 (2012) 211103.
[10] H.Y. Kim, J.H. Kim, Y.J. Kim, K.H. Chae, C.N. Whang, J.H. Song, S. Im, Opt. Mater. 17 (2001) 141.
[11] J.Y. Zhang, Y.X. Chen, T.L. Guo, Z.X. Lin, T.H. Wang, Nanotechnology 18 (2007) 325603.
[12] D. Shao, M. Yu, J. Lian, S. Sawyer, Appl. Phys. Lett. 102 (2013) 021107.
[13] G. Wang, X. Sun, F. Lu, H. Sun, M. Yu, W. Jiang, C. Liu, J. Lian, Small 8 (2012) 452.
[14] P.R. Bueno, F.M. Pontes, E.R. Leite, L.O.S. Bulhões, P.S. Pizani, P.N. Lisboa-Filho, W.H. Schreiner, J. Appl. Phys. 96 (2004) 2102.
[15] F. Zheng, M. Guo, M. Zhang, Cryst. Eng. Comm. 15 (2013) 277.
[16] R. Schaub, E. Wahlstrom, A. Ronnaus, E. Laegsgaard, I. Stensgaard, F. Besenbacher, Science 299 (2003) 377.
[17] D. Shao, H. Sun, M. Yu, J. Lian, S. Sawyer, Nano Lett. 12 (2012) 5840.
[18] D. Shao, L. Qin, S. Sawyer, Opt. Mater. 35 (2013) 563.
[19] D. Shao, M. Yu, H. Sun, T. Hu, J. Lian, S. Sawyer, Nanoscale 5 (2013) 3664.
[20] Y.Z. Jin, J.P. Wang, B.Q. Sun, J.C. Blakesley, N.C. Greenham, Nano Lett. 8 (2008) 1649.